BNL-211568-2019-JAAM

Ultrathin Visible-light Driven Mo–incorporation In2O3-ZnIn2Se4 Z-scheme Nanosheet Photocatalysts

Y. Chao, D. Su

To be published in "Advanced Materials"

February 2019

Center for Functional Nanomaterials

Brookhaven National Laboratory

U.S. Department of Energy

USDOE Office of Science (SC), Basic Energy Sciences (BES) (SC-22)

DISCLAIMER

Ultrathin Visible-light Driven Mo–incorporation In_2O_3-$ZnIn_2Se_4$ Z-scheme Nanosheet Photocatalysts

*Yuguang Chao, Peng Zhou, Na Li, Jianping Lai, Yong Yang, Yelong Zhang, Yonghua Tang, Wenxiu Yang, Yaping Du, Dong Su, Yisheng Tan, and Shaojun Guo**

Y. Chao, Dr. P. Zhou, Dr. J. Lai, Dr. Y. Yang, Dr. Y. Zhang,Y. Tang, Dr. W. Yang, Prof. S. Guo
Department of Materials Science and Engineering, College of Engineering, Peking University, Beijing 100871, China
E-mail: guosj@pku.edu.cn

Y. Chao, Prof. Y. Tan
State Key Laboratory of Coal Conversion, Institute of Coal Chemistry, Chinese Academy of Sciences, Taiyuan, 030001, China.

Dr. J. Lai, Prof. S. Guo
BIC-ESAT, College of Engineering, Peking University, Beijing 100871, China.

Y. Chao
University of Chinese Academy of Sciences, Beijing, 100049, P. R. China.

N. Li, Dr. D. Su
Center for Functional Nanomaterials, Brookhaven National Laboratory, Upton, New York 11973, United States.

Prof. Y. Du
School of Materials Science and Engineering & National Institute for Advanced Materials, Nankai University, Tianjin 300350, China.

Keywords: Z-scheme; nanosheets; $ZnIn_2Se_4$; photocatalysis

Abstract: Inspired by natural photosynthesis, the design of new Z-scheme photocatalytic systems is very promising for boosting the photocatalytic performance of H_2 production and CO_2 reduction, however, till now the direct synthesis of efficient Z-scheme photocatalysts remains a grand challenge. Herein, we demonstrate an interesting Z-scheme photocatalyst can be constructed by coupling In_2O_3 and $ZnIn_2Se_4$ semiconductors based on the theoretical calculations. Experimentally, we make a class of ultrathin In_2O_3-$ZnIn_2Se_4$ (donated as In_2O_3-ZISe) spontaneous Z-scheme nanosheet photocatalysts for greatly enhancing the photocatalytic H_2 production. Furthermore, we incorporate Mo atoms to the Z-scheme In_2O_3-ZISe nanosheet photocatalyst by forming Mo-Se bond, confirmed by X-Ray photoelectron spectroscopy, in which the formed $MoSe_2$ works as co-catalyst of Z-scheme photocatalyst. As a consequence, such unique structure of In_2O_3-ZISe-Mo makes it exhibit 21.7 and

232.6 times higher photocatalytic H_2 evolution activity than those of In_2O_3-$ZnIn_2Se_4$ nanosheet and In_2O_3 nanosheets, respectively. And In_2O_3-ZISe-Mo is also very stable for photocatalytic H_2 production by showing almost no activity decay for 16 h test. The ultraviolet-visible diffuse reflectance spectra, photoluminescence spectroscopy, transient photocurrent spectra and electrochemical impedance spectroscopy reveal that the enhanced photocatalytic performance of In_2O_3-ZISe-Mo is mainly attributed to its widened photoresponse range and effective carrier separation because of its special structure.

Photocatalytic water splitting to hydrogen is an ideal mean for renewable energy by overcoming the energy crisis caused by the overuse of fossil fuels and serious environmental issues.[1-5] *Yet*, to date, the reported photocatalysts still suffer from a quite low photoconversion efficiency, far below to satisfy the needs of practical applications. The low efficiency for photocatalytic water spillting can be primarily subjected to the following three reasons: (1) the majority of photocatalysts mainly absorb ultraviolet light, only 4% radiated to the earth's surface by sunlight; (2) the undesirable separation and transfer efficiency of photogeneration charge carriers over photocatalysts;[6] (3) the photocatalysts usually possess sluggish kinetics for H_2 evolution.[7] Thereby, designing and constructing a photocatalyst to improve the visible light harvesting, separation/transport efficiency of charge carriers and kinetics for water reduction is highly desirable. Inspired by nature photosynthesis,[8] multifarious all-solid-state artificial Z-scheme photocatalytic systems have been designed based on two semiconductors, which possess well matched band structures.[9-19] The special electronic transfer paths make these constructions not only maintain the sufficient energy levels of the photo-generation electrons and holes, but also offer broad light absorption and spatial separation of charge carriers, which are important for achieving more efficient photocatalysis.[20,21] However, to date, most of the reported Z-scheme photocatalysts systems still suffer from low charge transfer efficiency from body to the surface of catalyst.

2D nanosheets with high specific surface area, abundant catalytically active sites and shorter diffusion length of charge carriers are stimulating a wide range of interests in heterogeneous photocatalysis.[22-24] Metal chalcogenides (such as In_2S_3,[25] In_2Se_3,[26] ZnSe,[27] $ZnIn_2S_4$[28-30] and $CdIn_2S_4$[31]) with two-dimension geometric structure are of significance in acting as visible light-response photocatalysts with unique and tunable electronic structure for boosting photocatalytic water splitting. Consequently, 2D metal chalcogenide semiconductor photocatalysts have aroused diverse interests in photocatalytic H_2 evolution,[30] CO_2 fixation[29,31] and organic pollutants degradation[32]. In addition, the kinetics for water reduction at the interface of catalyst surface and electrolyte is also a crucial factor in restricting hydrogen evolution. Elemental incorporation with controllable surface engineering may realize the synergistic modulations of both active sites and adsorption or desorption for efficient HER performance,[33] however, achieving such target is still a great challenge although it is very important for further boosting the photocatalysis.

Herein, we first dexterously design and synthesize a class of In_2O_3-ZISe hetero-structured spontaneous Z-scheme nanosheet photocatalysts for greatly boosting the photocatalytic H_2 production. By further incorporating Mo atoms (acting as co-catalyst) to the Z-scheme In_2O_3-ZISe nanosheet photocatalyst, we demonstrate the resultant In_2O_3-ZISe-Mo can exhibit further enhanced photocatalytic performance for H_2 production, in which the H_2 production rate can be as high as 6.95 mmol g^{-1} h^{-1} under visible light, 21.7 and 232.6 times higher than those of In_2O_3-$ZnIn_2Se_4$ nanosheet and In_2O_3 nanosheets, respectively. And In_2O_3-ZISe-Mo exhibits high stability for photocatalytic H_2 production, revealed by the fact that photocatalytic activity can be well maintained for 16 h test. A series of characterization techniques such as ultraviolet-visible diffuse reflectance spectra, photoluminescence spectroscopy, transient photocurrent spectra and electrochemical impedance spectroscopy reveal that the unique structure of In_2O_3-ZISe-Mo is the key in contributing to the enhanced photocatalysis.

The electronic properties of In_2O_3 and $ZnIn_2Se_4$ were first investigated by density functional theory (DFT). **Figure 1a**&**1b** show the molecular structures of In_2O_3 and $ZnIn_2Se_4$, respectively, and the corresponding band structures are shown in **Figure S1**. The calculated results show that the conduction-band bottom of In_2O_3 mainly consists of In 5s and O 2p states and the valence-band top consists of O 2p state (**Figure 1c**&**1d**). In the $ZnIn_2Se_4$ model, the conduction-band bottom and the valence-band top of $ZnIn_2Se_4$ both consist of In 5s and Se 4p states (**Figure 1e**&**1f**). Due to the different electronic states, the valence-band top of $ZnIn_2Se_4$ is more positive than that of In_2O_3. This means that the In_2O_3 owns a strong oxidizing ability in the photocatalytic reaction. However, their conduction-band bottoms are nearly located in a same region. Hence, it can be speculated that In_2O_3 and $ZnIn_2Se_4$ in the In_2O_3-ZISe system can act as the oxidizing and reducing regions, respectively.

The In_2O_3-ZISe Z-scheme nanosheets were synthesized by the solvothermal reaction of $Zn(NO_3)_2 \cdot 6H_2O$, $In(NO_3)_3 \cdot xH_2O$ and Na_2SeO_3 in a mixed solution (35 mL) with a volume ratio of water/diethylenetriamine/$N_2H_4 \cdot H_2O$ = 3:3:1 at 160 °C for 12 h (Supporting Information, SI). The Field-emission scanning electron microscopy (FESEM) (**Figure 2a**&**S2**) and transmission electron microscopy (TEM) images (**Figure 2b**&**2c**) show that the product is dominated with uniform well-shaped 2D nanosheets with the average size of about 100-200 nm. The thickness of ultrathin In_2O_3-ZISe nanosheets is determined to be about 2.5-2.8 nm by atomic force microscope (AFM) (**Figure 2d**&**2e**). High-resolution TEM (HRTEM) image of In_2O_3-ZISe Z-scheme nanosheets reveals they have the lattice fringes lattice spaces of 0.293 nm and 0.33 nm, assigned to (222) crystal plane of stilliete In_2O_3 and $ZnIn_2Se_4$, respectively (**Figure 2f**&**S3**). The powder X-ray diffraction (XRD) patterns (**Figure S4**) clearly show the existence of stilliete In_2O_3 (JCPDS No. 06-0416) and $ZnIn_2Se_4$ (JCPDS No. 39-1156) in the nanosheets, being in accordance with the result from HRTEM image. Elemental mappings of In_2O_3-ZISe nanosheets reveal the well-distributed of Zn, In, and Se in the whole nanosheets (**Figure 2g**).

The Mo atoms were incorporated into In_2O_3-ZISe nanosheets in the form of Mo-Se bond for obtaining the Z-scheme In_2O_3-ZISe Z-scheme nanosheets with Mo as co-catalyst, through the solvothermal reaction with In_2O_3-ZISe nanosheets and Na_2MoO_4 as precursors at 200 °C for 12 h. The as-prepared product can still keep the feature of ultrathin nanosheets, and there is no obvious change in the size of nanosheets (**Figure S5**&**S6**), however, their surface becomes rough (**Figure 3a**&**3b**). The elemental mapping analysis further reveals the homogeneous distribution of Zn, In, Se and Mo elements in the In_2O_3-ZISe-Mo, confirming the incorporation of Mo atoms in the In_2O_3-ZISe hetero-structure nanosheets (**Figure 3c**). X-Ray photoelectron spectroscopy (XPS) measurement of In_2O_3-ZISe-Mo reveals the formation of Mo-Se bond (**Figure S7a**), in which the Mo $3d_{5/2}$ peak located at a binding energy of 228.3 eV matches well with that of $MoSe_2$,[34] and the Se 3d peak moves to high binding energy (**Figure S7b**).[35] Meanwhile, the In 3d peak also shifts to high binding energy while the Zn 3d peak has little shift (**Figure S7c** and **S7d**), indicating that the Mo atoms are bonded with $ZnIn_2Se_4$ phase. In addition, the other transition metals (Fe, Co, Ni) could also be incorporated into In_2O_3-ZISe nanosheets by the same method in the form of M-Se bond (**Figure S8**).

To shed light on the advantage of the synthesized Z-scheme system, the photocatalytic hydrogen evolution activities of both In_2O_3 nanosheets (**Figure S9**) and In_2O_3-ZISe hybrids nanosheets (with different mole ratio of In_2O_3 and $ZnIn_2Se_4$, **Figure S10**) were evaluated in aqueous solution containing 0.35 M Na_2S and 0.25 M Na_2SO_3 under visible light irradiation (λ>420 nm) by a 300 W Xe lamp without loading any co-catalyst. The effect of mole ratio of In_2O_3 to $ZnIn_2Se_4$ in the Z-scheme system for photocatalytic hydrogen production was first investigated (**Figure 4a).** The result shows that the optimal ratio of In_2O_3 to $ZnIn_2Se_4$ at 1:1 can lead to the highest photocatalytic HER activity. The H_2-evolution rate of the optimized In_2O_3-ZISe Z-scheme nanosheets is up to 319.7 umol g^{-1} h^{-1}, 10.70 times higher than that of In_2O_3 (29.9 umol g^{-1} h^{-1}), indicating the greatly enhanced catalytic activity of Z-scheme In_2O_3-ZISe nanosheets photocatalysts. By incorporating Mo element into In_2O_3-ZISe nanosheets by forming Mo-Se bonds, the photocatalytic hydrogen evolution activity

of the resultant In_2O_3-ZISe-Mo nanosheets can reach to 6.95 mmol g^{-1} h^{-1}, which is 21.7 times higher than that of the Z-scheme In_2O_3-ZISe nanosheets (**Figure 4b**). This photocatalyst is also comparable to or even better than those of most of the state-of-art catalysts reported previously (**Table S1**). In addition, we have also investigated the performance of photocatalytic H_2 evolution by incorporating other transition metals (Fe, Co, Ni). In_2O_3-ZISe-Ni has a comparable activity with In_2O_3-ZISe-Mo, whereas In_2O_3-ZISe-Fe shows poor activity for H_2 evolution. The order of photoactivity follows In_2O_3-ZISe-Mo > In_2O_3-ZISe-Ni > In_2O_3-ZISe-Co> In_2O_3-ZISe-Fe (**Figure S11**).

We have also studied the effect of sacrificial agent concentration on hydrogen production (**Table S2**). The lower concentration of sacrificial agent can not sacrifice the hole efficiently, resulting in lower activity. 0.25 M Na_2S/0.35 M Na_2SO_3 is an optimal concentration for effective hydrogen production and economic perspective. We further studied the photocatalytic stability of the In_2O_3-ZISe-Mo and In_2O_3-ZISe nanosheets. There are negligible drops in the rates of hydrogen evolution during four consecutive cycles with accumulatively 16 h under the irradiation of visible light (**Figure 4c**&**S12**). Furthermore, there are almost no composition changes (**Figure S13**) and retain the overall structure (**Figure S14**) after stability test, further suggesting the excellent stability of ultrathin In_2O_3-ZISe-Mo Z-scheme nanosheets.

To confirm the enhanced hydrogen evolution activity of In_2O_3-ZISe-Mo and In_2O_3-ZISe, we conducted a thoroughly characterization of the new Z-scheme system photocatalyst. First, ultraviolet-visible diffuse reflectance spectra were utilized to determine the light-harvesting capability of the as-prepared In_2O_3 and In_2O_3-ZISe nanosheets. As depicted in **Figure 4d**, the absorption edge of In_2O_3 is determined to be 410 nm, while the In_2O_3-ZISe hybrid nanosheets show the obviously broadened optical absorption extending to 600 nm. The red-shift of absorption edge is benefit for utilizing the visible light. The band gap energy (E_g) can be calculated on the basis of the ultraviolet-visible diffuse reflectance spectra.[36] The band gap of In_2O_3-ZISe ultrathin nanosheets (inset of **Figure 4d**) is calculated to be about 2.73 eV, much narrower than that of In_2O_3 (2.98 eV),

being in agreement with the DFT calculation result. In addition, the small band gap of In_2O_3-ZISe can broaden the light harvesting, and the photo-excited electron-hole pairs can trigger the redox reactions.

XPS valence band spectroscopy were performed to determine the valence band (VB) positions of the as-prepared In_2O_3 and In_2O_3-ZISe nanosheets (**Figure 4e**), showing that the VB positions of In_2O_3 and In_2O_3-ZISe nanosheets are 2.28 eV and 1.32 eV, respectively. Therefore, the corresponding conduction band (CB) positions of as-prepared samples were obtained by coupling the VB positions and optical band gaps. And the CB positions of In_2O_3-ZISe nanosheets up-shift by about 0.71 eV with respect to that of the prepared In_2O_3 nanosheets. Based on the above result, the energy band alignment between In_2O_3 and In_2O_3-ZISe is shown in **Figure 4f**, forming a valid Z-scheme photocatalyst system, being in well consistent with the DFT calculation result.

In order to further explore the reason for high photocatalytic hydrogen production performance of In_2O_3-ZISe Z-scheme nanosheets photocatalyst system, we performed the photoelectrochemical characterization. First, the steady-state photoluminescence (PL) spectroscopy was carrying out to disclose the separation of photo-generation electron-hole pairs. **Figure 5a** shows the photoluminescence spectra of In_2O_3 and In_2O_3-ZISe Z-scheme nanosheets. Apparently, the emission of In_2O_3-ZISe is strongly quenched compared with that of the In_2O_3 nanosheets, indicating that the recombination of photo-generation electron–hole pairs in In_2O_3-ZISe nanosheets was forcefully suppressed by forming the Z scheme due to the rapid separation of charge carrier between the contacted interfaces. In addition, the incorporation of Mo atoms could further reduce the intensity of PL (**Figure 5a**), implying that Mo atom was an efficient electronic capture center. Meanwhile, the time-resolved photoluminescence spectroscopy (TRPL) was employed to elaborate the specific charge carrier dynamics of In_2O_3 and In_2O_3-ZISe hybrid nanosheet (**Figure 5b**). Obviously, the average emission lifetime of In_2O_3 nanosheets (5.3 ns) is prolonged to 6.5 ns after forming the In_2O_3-ZISe Z-scheme photocatalyst system. Therefore, the efficient separation and migration of interfacial

charge carriers were achieved in In_2O_3-ZISe hybrid nanosheet. On the other hand, comparing with In_2O_3-ZISe, the emission lifetime become much longer when the Mo is incorporated (**Figure 5b**), being consistent with the result from steady-state photoluminescence. Moreover, as a powerful technology, transient photocurrent spectra clearly show that In_2O_3-ZISe nanosheet displays a remarkably enhanced photocurrent than In_2O_3 nanosheet (**Figure 5c**), revealing the promoted separation and transfer of the photo-generated charge carriers in the In_2O_3-ZISe Z-scheme photocatalyst system, and In_2O_3-ZISe-Mo can further enhance the separation of electron-hole pairs.

The electrochemical impedance spectroscopy (EIS) is also considered as an important tool for characterizing the separation of photo-generation charge carriers. The EIS (**Figure 5d**) reveals that the In_2O_3-ZISe-Mo exhibits the smallest semicircle in Nyquist plots, thereby, the lowest charge transfer resistance, permitting fast separation and transport of photo-generation electron-hole pairs. All above results demonstrate that the constructed In_2O_3-ZISe-Mo Z-scheme nanosheets can enhance the light absorption, separation and transfer of photo-generation charge carriers and optimize the kinetic for water reduction, thus resulting in high-efficiency photocatalytic water reduction.

In summary, we theoretically and experimentally demonstrate a new class of spontaneous Z-scheme In_2O_3-ZISe photocatalytic system. When the Mo atoms were further incorporated to the In_2O_3-ZISe Z-scheme nanosheets in the form of Mo-Se bond, the resultant In_2O_3-ZISe-Mo nanosheets can integrate the advantage of Z-scheme catalysts and co-catalyst. As a result, they exhibit a very high H_2 evolution rate of 6.95 mol g^{-1} h^{-1}, much better than the In_2O_3-ZISe and In_2O_3 nanosheets (the rates are 319.7 umol g^{-1} h^{-1} and 29.9 umol g^{-1} h^{-1}, respectively). They also show high durability for hydrogen evolution photocatalysis by showing almost no activity decrease after 16 test. The UV-Vis diffuse reflectance spectra of the In_2O_3-ZISe-Mo nanosheets show they can broaden the absorption of light, and their PL spectroscopy, transient photocurrent spectra and EIS reveal they can promote the separation of photo-generation charge carriers, both of which are the key in greatly promoting the hydrogen evolution photocatalysis herein.

Supporting Information
Supporting Information is available from the Wiley Online Library or from the author.

Acknowledgements
This work was financially supported by the National Key R&Development Program of China (No. 2016YFB0100201), National Natural Science Foundation of China (51671003 and 21802003), BIC-ESAT funding and China Postdoctoral Science Foundation (No. 2017M620494 and 2018M631239). This research used resources of the Center for Functional Nanomaterials, which is a U.S. DOE Office of Science Facility, at Brookhaven National Laboratory under Contract No. DE-SC0012704.

Received: ((will be filled in by the editorial staff))
Revised: ((will be filled in by the editorial staff))
Published online: ((will be filled in by the editorial staff))

References

[1] K. Maeda, K. Teramura, D. Lu, T. Takata, N. Saito, Y. Inoue, K. Domen, *Nature* **2006**, 7082, 295.
[2] K. K. Sakimoto, A. B. Wong, P. Yang, *Science* **2016**, 351, 74-77.
[3] X. Meng, L. Liu, S. Ouyang, H. Xu, D. Wang, N. Zhao, J. Ye, *Adv. Mater.* **2016**, 32, 6781.
[4] Y. Zhang, Z. Mu, C. Yang, Z. Xu, S. Zhang, X. Zhang, Y. Li, J. Lai, Z. Sun, Y. Yang, Y. Chao, C. Li, X. Ge, W. Yang, S. Guo, *Adv. Funct. Mater.* **2018**, 1707578.
[5] P. Zhou, J. Lai, Y. Tang, F. Lin, Y. Chao, S. Guo, *Appl. Catal. B: Environ.* **2018**, 238, 161-167.
[6] Y. Xu, Y. Ye, T. Liu, X. Wang, B. Zhang, M. Wang, H. Han; C. Li, *J. Am. Chem. Soc.* **2016**, 34, 10726.
[7] J. Ran, G. Gao, F. T. Li, T. Y. Ma, A. Du, S. Z. Qiao, *Nat. Commun.* **2017**, 13907.
[8] A. J. Bard, *J. Photochem.* **1979**, 10, 59-75.
[9] Q. Wang, T. Hisatomi, Q. Jia, H. Tokudome, M. Zhong, C. Wang, Z. Pan, T. Takata, M. Nakabayashi, N. Shibata, Y. Li, I. D. Sharp, A. Kudo, T. Yamada, K. Domen, *Nat. Mater.* **2016**, 6, 611.
[10] H. Tada, T. Mitsui, T. Kiyonaga, T. Akita, K. Tanaka, *Nat. Mater.* **2006**, 10, 782.
[11] P. Zhou, J. Yu, M. Jaroniec, *Adv. Mater.* **2014**, 29, 4920.
[12] H. Li, W. Tu, Y. Zhou, Z. Zou, *Adv. Sci.* **2016**, 11, 1500389.
[13] Q. Yuan, D. Liu, N. Zhang, W. Ye, H. Ju, L. Shi, R. Long, J. Zhu, Y. Xiong, *Angew. Chem., Int. Ed.* **2017**, 15, 4206.
[14] M. Zhu, Z. Sun, M. Fujitsuka, T. Majima, *Angew. Chem., Int. Ed.* **2018**, 8, 2160.
[15] K. Iwashina, A. Iwase, Y. H. Ng, R. Amal, A. Kudo, *J. Am. Chem. Soc.* **2015**, 2, 604.
[16] K. Maeda, *ACS Catal.* **2013**, 3, 1486.
[17] Z. Zhang, J. Huang, Y. Fang, M. Zhang, K. Liu, B. Dong, *Adv. Mater.* **2017**, 18, 1606688.
[18] X. Guan, L. Guo, *ACS Catal.* **2014**, 9, 3020.
[19] Y. Kim , D. Shin , W. J. Chang , H. L. Jang , C. W. Lee , H.-E. Lee , K. T. Nam, *Adv. Funct. Mater.* **2015**, 25, 2369.
[20] S. Bai, J. Jiang, Q. Zhang, Y. Xiong, *Chem. Soc. Rev.* **2015**, 10, 2893.
[21] X. Zhang, Z. Zhang, D. Wu, X. Zhang, X. Zhao, Z. Zhou, *Small methods* **2018**, 2, 1700359.
[22] L. Wang, Y. Zhang, L. Chen, H. Xu, Y. Xiong, *Adv. Mater.* **2018**, e1801955.
[23] J. Di, J. Xiong, H. Li, Z. Liu, *Adv. Mater.* **2018**, 1.

[24] Z. Sun, N. Talreja, H. Tao, J. Texter, M. Muhler, J. Strunk, J. Chen, *Angew. Chem., Int. Ed.* **2017**.
[25] K. H. Park, K. Jang, S. U. Son, *Angew, Chem., Int. Ed.* **2006**, 28, 4608.
[26] D. Wei, Z. Lin, Z. Cui, S. Su, D. Zhang, M. Cao, C. Hu, *Chem. Commun.* **2013**, 83, 9609.
[27] X. Wu, Y. Yu, Y. Liu, Y. Xu, C. Liu, B. Zhang, *Angew. Chem., Int. Ed.* **2012**, 13, 3211.
[28] Z. Lei, W. You, M. Liu, G. Zhou, T. Takata, M. Hara, K. Domen, C. Li, *Chem. Commun.* **2003**, 17, 2142.
[29] X. Jiao, Z. Chen, X. Li, Y. Sun, S. Gao, W. Yan, C. Wang, Q. Zhang, Y. Lin, Y. Luo, Y. Xie, *J. Am. Chem. Soc.* **2017**, 22, 7586.
[30] W. Yang, L. Zhang, J. Xie, X. Zhang, Q. Liu, T. Yao, S. Wei, Q. Zhang, Y. Xie, *Angew. Chem., Int. Ed.* **2016**, 23, 6716.
[31] S. Wang, B. Y. Guan, Y. Lu, X. W. D. Lou, *J. Am. Chem. Soc.* **2017**, 48, 17305.
[32] X. Tu, J. Lu, M. Li, Y. Su, G. Yin, D. He, *Nanoscale* **2018**, 10, 4735.
[33] Y. Chao, J. Zheng, H. Zhang, F. Li, F. Yan, Y. Tan, Z. Zhu, *Chem. Eng. J.* **2018**, 281.
[34] F. Gustavsson, S. Jacobson, A. Cavaleiro, T. Polcar, *Wear* **2013**, 1-2, 286.
[35] L. Assmann, J. C. Bernède, A. Drici, C. Amory, E. Halgand, M. Morsli, *Appl. Sur. Sci.* **2005**, 1-3, 159.
[36] X. She, J. Wu, H. Xu, J. Zhong, Y. Wang, Y. Song, K. Nie, Y. Liu, Y. Yang, M.-T. F. Rodrigues, R. Vajtai, J. Lou, D. Du, H. Li, P. M. Ajayan, *Adv. Energy Mater.* **2017**, 7, 1700025.

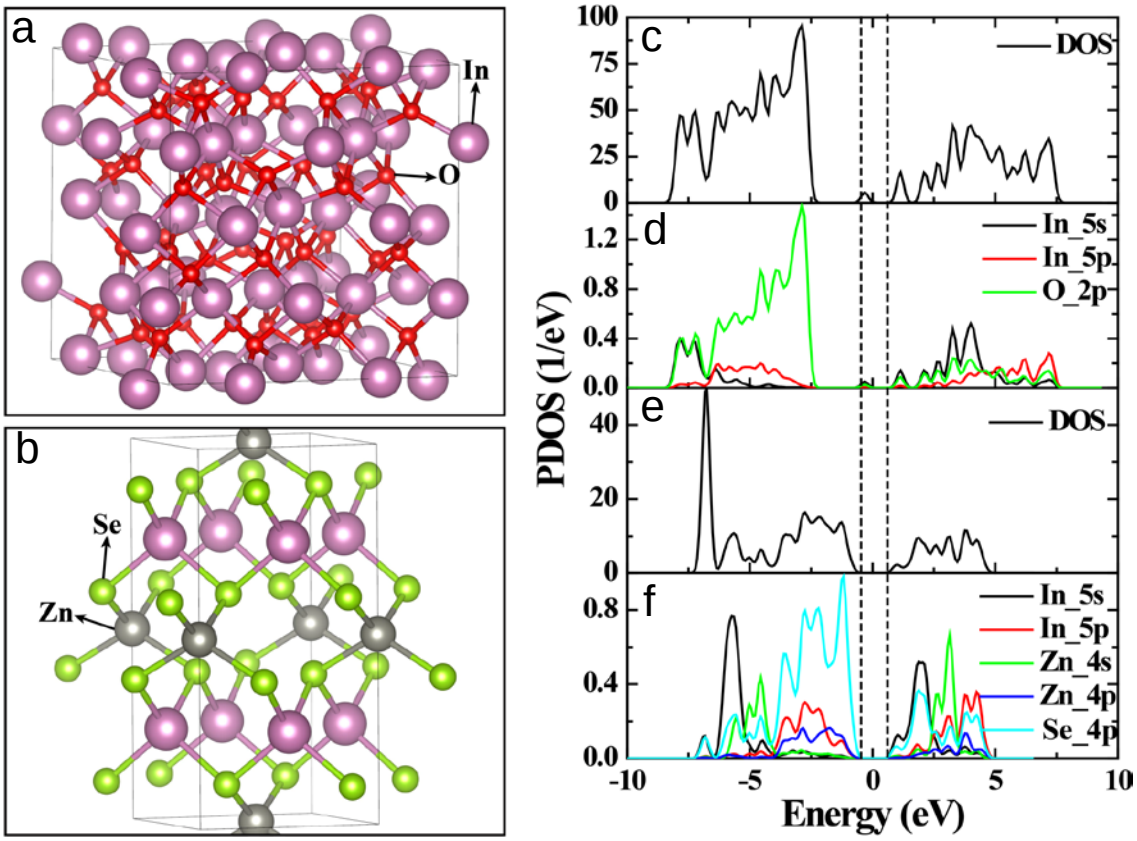

Figure 1. Optimized geometry structures of (a) In_2O_3 and (b) $ZnIn_2Se_4$ and (c-f) the corresponding density of state (DOS) plots. The dashed line stands for Fermi level. All electronic states were normalized by the deep In 4d states.

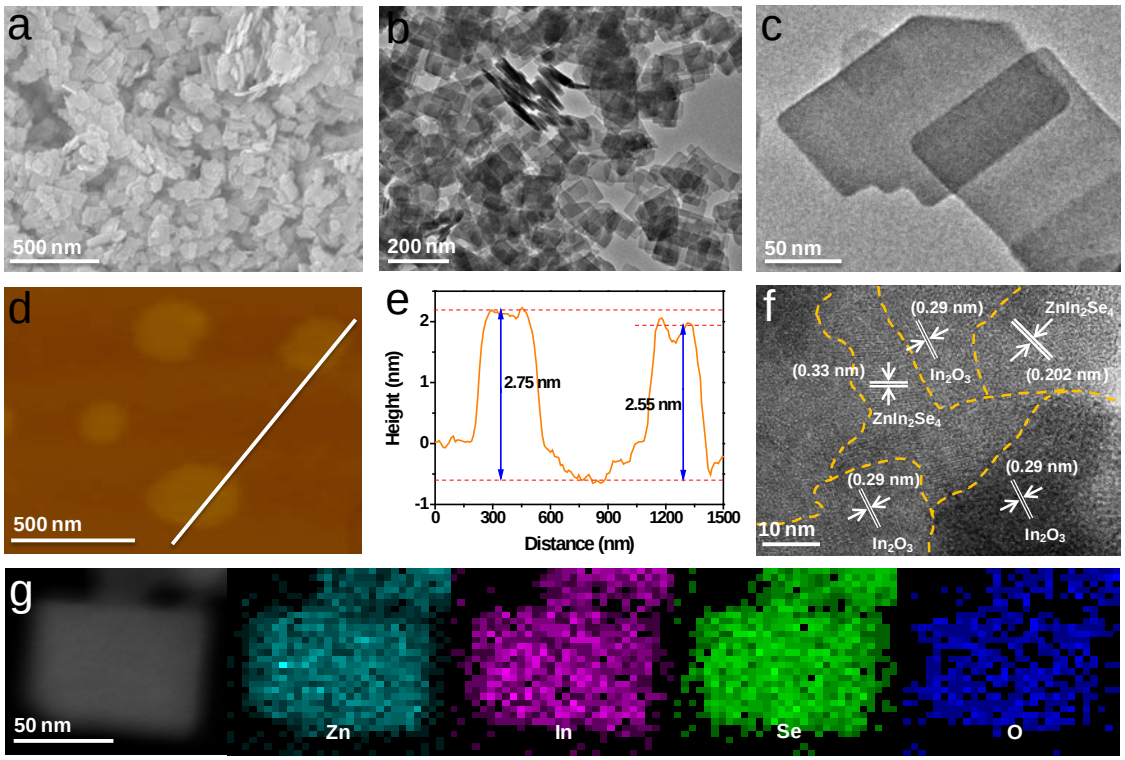

Figure 2. (a) SEM image, (b, c) TEM, (d) AFM, (e) height profile, (f) HRTEM and (g) element mapping of Zn, In, Se, O of In_2O_3-ZISe Z-scheme nanosheets.

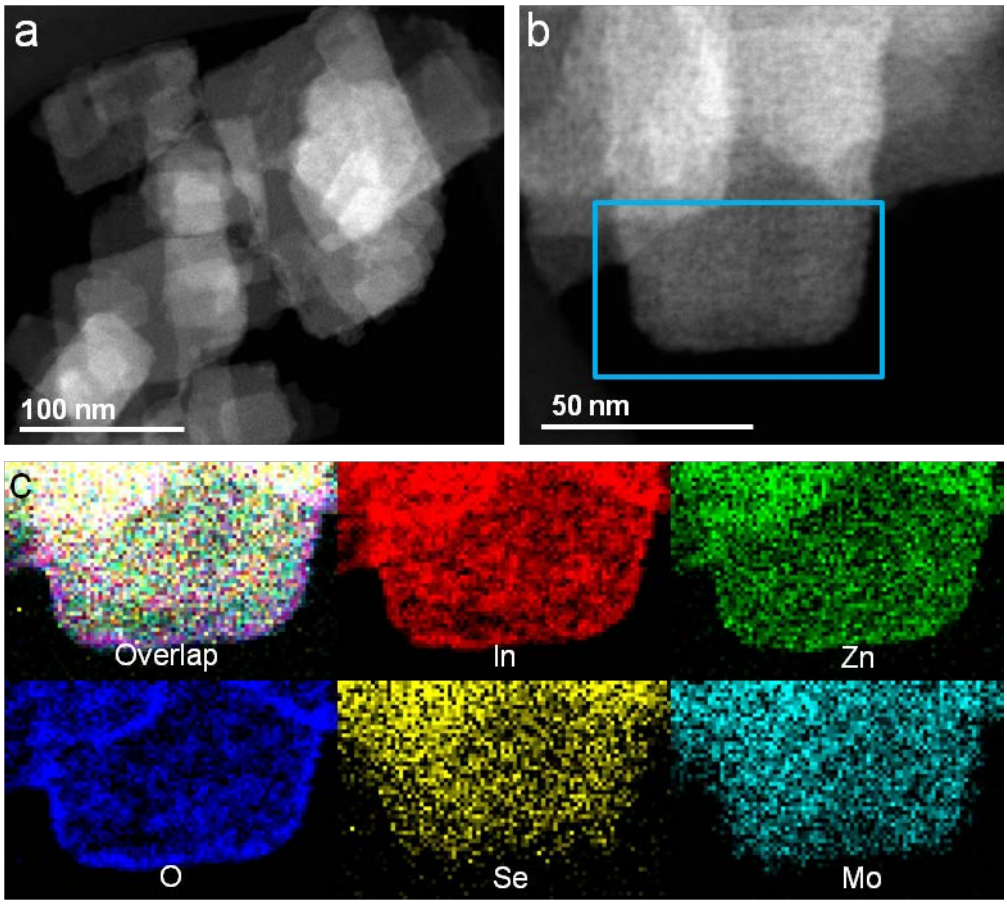

Figure 3. (a, b) STEM images and (c) elemental distribution of Zn, In, Se, O of as-made In_2O_3-ZISe-Mo Z-scheme nanosheets.

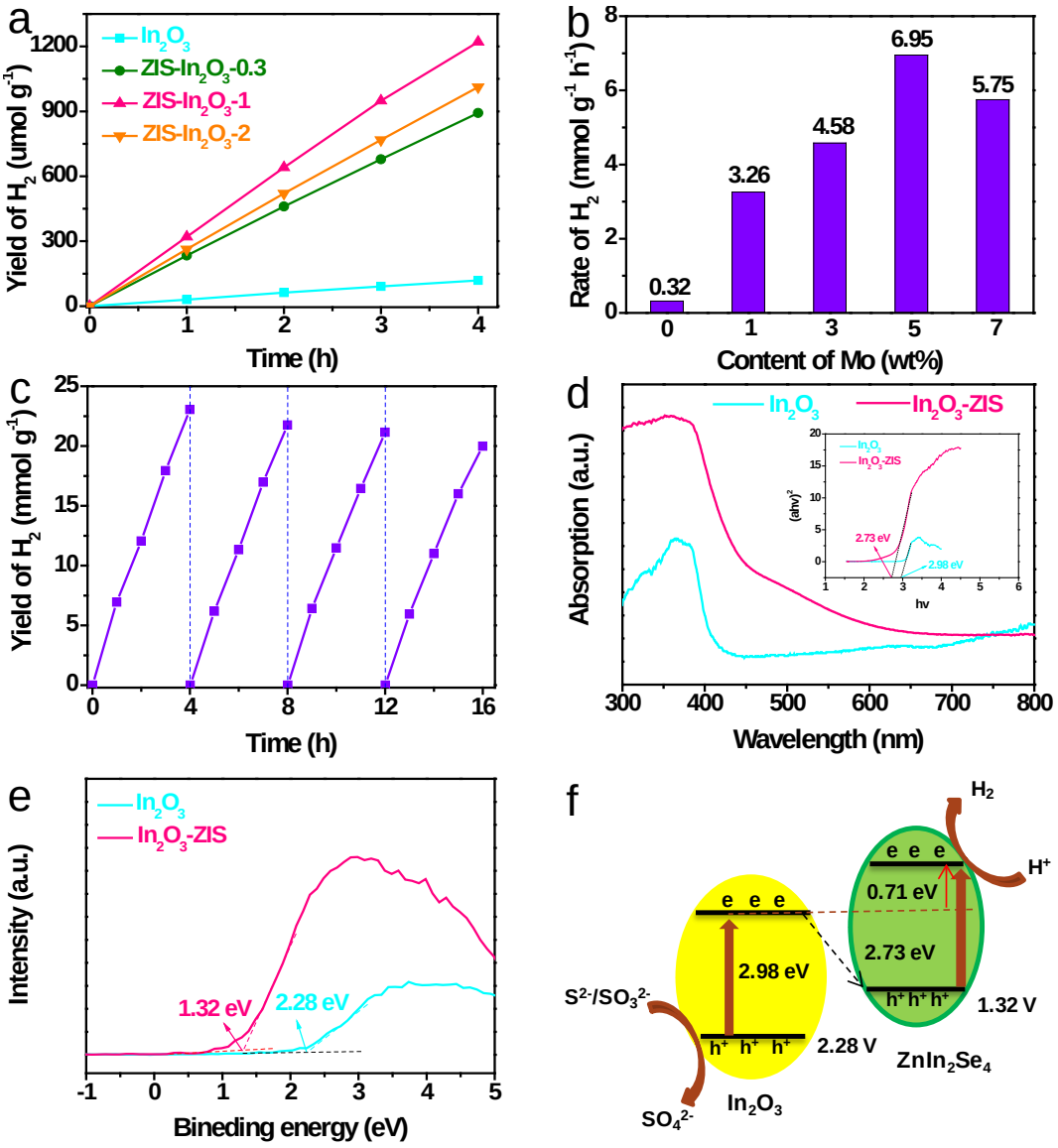

Figure 4. (a) Time course of H_2 evolution performance of various In_2O_3-ZISe nanosheets. (b) The rate of H_2 production over ultrathin In_2O_3-ZISe-Mo Z-scheme nanosheets with different Mo incorporation amounts. (c) Recycling performance of In_2O_3-ZISe-Mo nanosheets toward the photocatalytic H_2 production. (d) UV/Vis absorption spectra and band gap energies and (e) XPS valence spectrum of In_2O_3 and In_2O_3-ZISe samples. (f) Schematics of photocatalytic reaction processes for the In_2O_3-ZISe Z-schemce system.

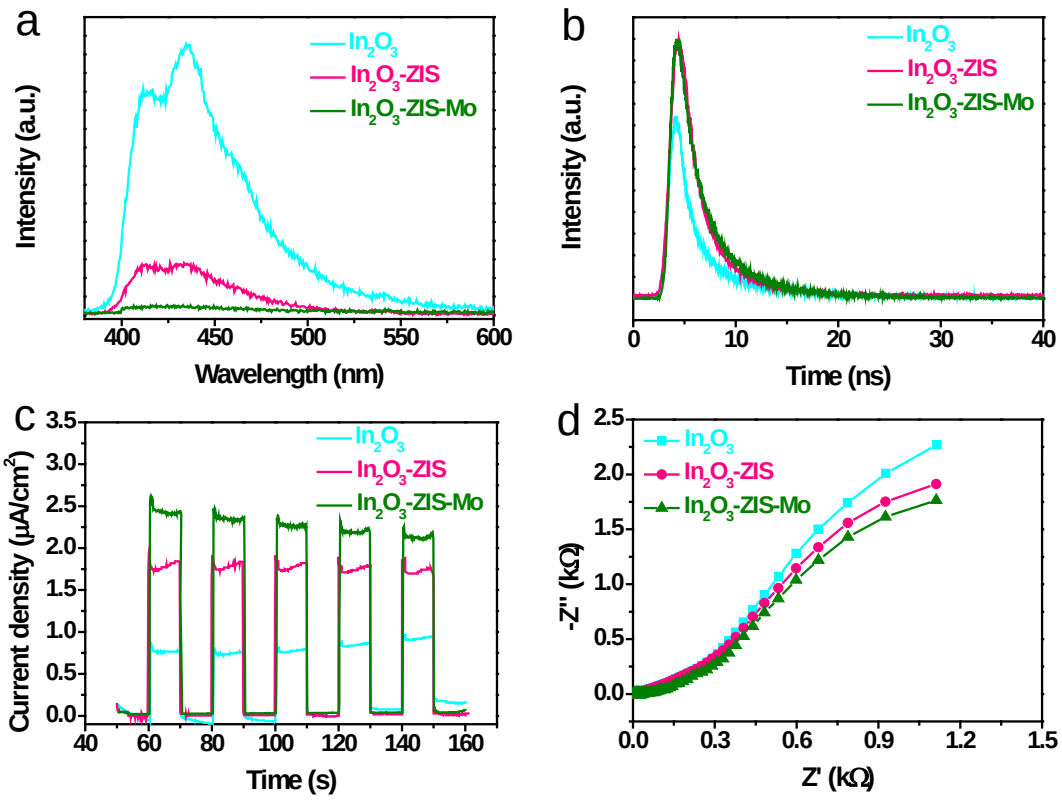

Figure 5. (a) Steady-state PL spectra, (b) time-resolved transient PL decay, (c) transient photocurrent spectra and (d) EIS spectra of In_2O_3, In_2O_3-ZISe and In_2O_3-ZISe-Mo.